

**Sequential and one-pot post-polymerization modification reactions of thiolactone-containing polymer brushes**

Journal:	<i>Polymer Chemistry</i>
Manuscript ID	PY-ART-07-2019-001123.R1
Article Type:	Paper
Date Submitted by the Author:	16-Aug-2019
Complete List of Authors:	Reese, Cassandra ; University of Southern Mississippi, School of Polymer Science and Engineering Thompson, Brittany; University of Southern Mississippi, School of Polymer Science and Engineering Logan, Phillip; University of Southern Mississippi, School of Polymer Science and Engineering Stafford, Christopher; National Institute of Standards and Technology, Polymers Division Blanton, Michael; University of Southern Mississippi, School of Polymer Science and Engineering Patton, Derek; University of Southern Mississippi, School of Polymers

## ARTICLE

## Sequential and one-pot post-polymerization modification reactions of thiolactone-containing polymer brushes

, 39Received 00th January 20xx,  
Accepted 00th January 20xx

Cassandra M. Reese,<sup>a</sup> Brittany J. Thompson,<sup>a</sup> Phillip K. Logan,<sup>a</sup> Christopher M. Stafford,<sup>b</sup> Michael Blanton,<sup>a</sup> and Derek L. Patton<sup>a\*</sup>

DOI: 10.1039/x0xx00000x

Thiolactone chemistry has garnered significant attention as a powerful post-polymerization modification (PPM) route to multifunctional polymeric materials. Here, we apply this versatile chemistry to the fabrication of ultrathin, multifunctional polymer surfaces via aminolysis and thiol-mediated double modifications of thiolactone-containing polymer brushes. Polymer brush surfaces were synthesized via microwave-assisted surface-initiated polymerization of DL-homocysteine thiolactone acrylamide. Aminolysis and thiol-Michael double modifications of the thiolactone-functional brush were explored using both sequential and one-pot reactions with bromobenzyl amine and 1*H*,1*H*-perfluoro-*N*-decyl acrylate. X-ray photoelectron spectroscopy and argon gas cluster ion sputter depth profiling enabled quantitative comparison of the sequential and one-pot PPM routes with regard to conversion and spatial distribution of functional groups immobilized throughout thickness of the brush. While one-pot conditions proved to be more effective in immobilizing the amine and acrylate within the brush, the sequential reaction enabled the fabrication of multifunctional, micropatterned brush surfaces using reactive microcontact printing.

### Introduction

A major thrust in polymer surface engineering is focused on strategies to deliberately tailor the composition, distribution, and spatial arrangement of functional groups on a surface using facile and efficient chemistries. Precise control over the aforementioned properties lead to their useful applications in antifouling coatings,<sup>1, 2</sup> biosensors,<sup>3, 4</sup> cell adhesive surfaces,<sup>5</sup> lithium ion batteries,<sup>6-8</sup> and surface wrinkling.<sup>9, 10</sup> Functionalized polymer brush surfaces have been prepared via grafting-to, grafting-through, or grafting-from. However, grafting-from, commonly referred to as surface-initiated polymerization (SIP), serves as a more attractive approach to synthesize dense polymer brushes with excellent control over parameters such as brush thickness, grafting density, composition, and architecture. Advances in SIP techniques have undoubtedly provided polymer chemists with tools to tailor these parameters given knowledge of reaction conditions, reactivity ratios, and order of monomer addition, but challenges remain particularly regarding direct polymerization of monomers with complex or highly reactive pendent functionality.<sup>11, 12</sup> Post-polymerization modification (PPM), when combined with SIP, has evolved as a powerful

approach to engineer polymer surfaces with complex functionality.<sup>13-15</sup> PPM is a process based on the polymerization of monomers carrying chemoselective handles that are inert under polymerization conditions, but can subsequently be converted into a broad range of functional groups using a variety of high efficacy reactions such as aminolysis of active esters, copper catalyzed azide-alkyne cycloaddition (CuAAC), Diels-Alder cycloadditions, nitroxide photoclick reactions, and thiol-based reactions.<sup>16, 17</sup> PPM enables the transformation of one reactive polymer brush scaffold into a library of functional homopolymer brush surfaces differing only in the chemical identity of pendent functionality of the repeat unit.<sup>13, 18</sup>

Brush surfaces expressing multiple functionalities can be achieved using a variety of post-polymerization processes involving simultaneous, sequential, or one-pot reactions. The simplest route to multifunctional surfaces involves simultaneous PPM of a reactive homopolymer brush scaffold with two or more modifiers – a route yielding brushes with a random distribution of functional groups along the polymer chains.<sup>19, 20</sup> Assuming each modifier exhibits similar reactivity towards the reactive brush, the modifier feed ratio provides a facile route to tailor functional group composition. For example, we previously demonstrated the synthesis of poly(propargyl methacrylate) brushes and sequential PPM via thiol-alkyne reactions using a library of thiols to selectively tune the surface properties.<sup>21</sup> Similarly, sequential, and in some cases, one-pot post-polymerization modifications of copolymer brush scaffolds carrying two or more pendent groups with orthogonal reactivity provides access to

<sup>a</sup> School of Polymer Science and Engineering, University of Southern Mississippi, Hattiesburg, MS 39406. E-mail: derek.patton@usm.edu

<sup>b</sup> Materials Science and Engineering Division, National Institute of Standards and Technology, Gaithersburg, MD 20899.

Electronic Supplementary Information (ESI) available: 1H and 13C NMR of monomer and additional XPS analysis.

See DOI: 10.1039/x0xx00000x

multifunctional brush surfaces. In contrast to the simultaneous PPM approach previously described, copolymerization parameters employed during SIP (e.g., co-monomer feed and reactivity ratios), rather than the PPM process, have been used to dictate final chemical composition of the modified brush.<sup>19–21</sup>

Furthermore, modification of brush surfaces can be exploited via a number of patterning techniques, such as microcontact stamping, microcapillary patterning, and photopatterning using sequential and orthogonal chemistries with high spatial resolution.

More recently, several post-polymerization modification strategies have emerged that target the design of multifunctional homopolymers, i.e., homopolymers bearing two distinct functional groups on every repeat unit. These strategies rely on either latent, chemoselective, or orthogonal reaction sites pendent to the monomer for sequential or simultaneous introduction of two functional groups per repeat unit following polymerization. Kubo et al.<sup>22, 23</sup> recently reviewed several innovative routes to multifunctional homopolymers; however, these synthetic strategies have not frequently been translated or adapted for functionalization of polymer brush surfaces. In one example, Lillethorup and coworkers<sup>24</sup> exploited the latent reactivity of epoxides on poly(glycidyl methacrylate) brushes to install two distinct redox moieties on every repeat unit. The epoxide was first ring-opened with sodium azide to yield a polymer brush with azide and alcohol functionality in each repeat unit. These functional groups enabled the synthesis of multifunctional homopolymer brushes bearing ferrocene and nitrobenzene redox active moieties using sequential CuAAC and isocyanate reactions. While Lillethorup et al.<sup>24</sup> demonstrated poly(glycidyl methacrylate) as an effective precursor for multifunctional homopolymer brushes, the approach requires three sequential PPM reactions to achieve the final brush surface and is not amendable to one-pot reactions.

In exploration of alternative routes to multifunctional homopolymer brush surfaces, we turned our attention to the efficient double modification strategy using  $\gamma$ -thiolactone reported by Du Prez et al.<sup>25–31</sup> Thiolactones undergo a nucleophilic ring-opening reaction with primary amines forming an amide between the carbonyl of the thiolactone, liberating a thiol that can undergo sequential thiol-coupling reactions with alkenes, alkynes, maleimides, or acrylates. Thiolactone double modification reactions exhibit 100 % atom-efficiency and can be performed in an efficient one-pot reaction. Furthermore, the latent thiol functionality obtained from the thiolactone is an attractive synthetic approach to design stable thiol-functionalized polymers. While Du Prez and others have demonstrated thiolactone chemistry for the versatile design of polymeric architectures, the chemistry has received surprising little attention in the context of surface modification.<sup>29, 31, 32</sup> To our knowledge, the thiolactone double modification strategy has yet to be exploited for synthesis of multifunctional homopolymer brush surfaces.

Herein, we demonstrate a versatile post-polymerization modification strategy (PPM) to synthesize multifunctional homopolymer brush surfaces based on poly(acrylamide-

homocysteine thiolactone) (pAHT). pAHT is synthesized via microwave-assisted surface-initiated radical polymerization ( $\mu$ W-SIP).<sup>33</sup> Modification of the brush surfaces with amines generates a reactive thiol precursor, which is available to undergo a sequential base-catalyzed thiol-Michael reaction with functional acrylates and maleimides. Additionally, we employ a one-pot double modification reaction to demonstrate the versatility of thiolactone chemistry as a powerful PPM platform for polymer brush surfaces. X-ray photoelectron spectroscopy (XPS) depth profile experiments provide key insights into the PPM efficiency (e.g. sequential versus one-pot reactions) of the pAHT brushes. Finally, we exploit reactive microcontact printing ( $\mu$ CP) with fluorescent post-modifiers to design multifunctional, micropatterned, fluorescent surfaces.

## Experimental Section

### Materials

Certain commercial equipment, instruments, or materials are identified in this paper in order to specify the experimental procedure adequately. Such identification is not intended to imply recommendation or endorsement by the National Institute of Standards and Technology, nor is it intended to imply that the materials or equipment identified are necessarily the best available for the purpose.

DL-homocysteine thiolactone hydrochloride (99 %) was purchased from Alfa Aesar and used as received. Triethylamine (TEA), 1,8-diazabicyclo(5.4.0)undec-7-ene (DBU), dansylcadaverine, and 4-bromobenzylamine (BBA) were purchased from Sigma-Aldrich and used as received. 1*H*,1*H*-Perfluoro-*N*-decyl acrylate (PFDA) was purchased from Gelest. Texas Red<sup>®</sup> C2 maleimide was purchased from Introgen. Silicon wafers (orientation <100>, native oxide) were purchased from University Wafer. The PDMS stamp (5  $\mu$ m lines spaced by 10  $\mu$ m) was purchased from Research Micro Stamps. An azo-based trichlorosilane initiator for surface-initiated polymerization was synthesized per literature procedures.<sup>34, 35</sup>

### Instrumentation and characterization

Ellipsometry measurements were carried out using a Gartner Scientific Corporation LSE ellipsometer with a 632.8 nm laser at 70° from the surface normal. Multiple thickness measurements were taken for each sample to determine the uncertainty in the measurements. Grazing angle attenuated total reflection Fourier transfer infrared (gATR-FTIR) analysis was carried out using a Thermo Scientific FTIR (Nicolet 8700) equipped with a VariGATR™ accessory (grazing angle 65°, germanium crystal; Harrick Scientific). Spectra were collected with a resolution of 4  $\text{cm}^{-1}$  by accumulating a minimum of 128 scans per sample. All spectra were collected while purging the VariGATR attachment and FTIR instrument with nitrogen along the infrared beam path to minimize the peaks corresponding to atmospheric water and CO<sub>2</sub>. Spectra were analyzed and processed using Omnic software. Static water contact angles (WCA) were measured using 6  $\mu$ L water droplets on a Rame-

hart goniometer. XPS and depth profile experiments were performed using a Thermo-Fisher ESCALAB Xi+ spectrometer equipped with a monochromatic Al X-ray source (1486.6 eV) and a MAGCIS Ar<sup>+</sup>/Ar<sub>n</sub><sup>+</sup> gas cluster ion sputter (GCIS) gun. Measurements were performed using the standard magnetic lens mode and charge compensation. The base pressure in the analysis chamber during spectral acquisition was at 3 × 10<sup>-7</sup> mBar. Spectra were collected at a takeoff angle of 90° from the plane of the surface. The pass energy of the analyzer was set at 150 eV for survey scans with an energy resolution of 1.0 eV; total acquisition time was 220 s. Binding energies were calibrated with respect to C 1s at 284.8 eV. Sputter depth profiling was performed by rastering an argon ion beam in cluster mode (6keV, Ar<sub>300</sub><sup>+</sup>) over a 2 mm<sup>2</sup> area at an angle 30° to the sample normal. To avoid crater edge effects, an X-ray spot size of 650 μm was employed. The X-ray gun was blanked during each argon sputtering step to minimize changes in composition due to x-ray exposure. All spectra were recorded using the Thermo Scientific Avantage software; data files were translated to VGD format and processed using the Thermo Avantage package v5.9904. Fluorescent microscopy was conducted on a Zeiss LSM 710 laser confocal scanning microscope running Zen Black software and a λ = 405 nm and 633 nm argon laser.

#### Cleaning of silicon wafers

Silicon wafers were cut into 1 cm × 1 cm pieces and cleaned using the RCA procedure to remove organic residue and oxidize the surface of the wafer. The general recipe for RCA cleaning is 5 parts deionized (DI) water, 1 part 27 % ammonium hydroxide, and 1 part 30 % hydrogen peroxide. DI water and ammonium hydroxide were added to a test tube and heated to 70 °C for 5 min, and then the test tube was removed from heat and hydrogen peroxide was added. The silicon wafers were transferred to the test tube and heated at 70 °C for 15 min. After 15 min, the wafer was removed from the solution and washed multiple times with DI water. Clean substrates were stored in an oven at 120 °C before initiator functionalization.

#### Immobilization of initiator onto silicon substrates

Clean, dry silicon substrates were transferred into a dry, septum sealed test tube containing a toluene solution of azo-initiator (4 mmol, 13 mL) and triethylamine (TEA) (0.2 mL). The immersion time was 1 h. Substrates were removed, rinsed with toluene, methanol, and DI water and dried under a stream of nitrogen. If not used immediately, initiator functionalized substrates were stored in the dark at -20 °C in toluene.

#### Synthesis of DL-homocysteine thiolactone acrylamide monomer

Thiolactone acrylamide monomer was synthesized following a procedure reported by Reinicke and coworkers.<sup>28</sup> An ice-cooled solution of DL-homocysteine thiolactone hydrochloride (5.0 g, 32.5 mmol) in H<sub>2</sub>O/1,4-dioxane (1/1, 70 mL) was treated with NaHCO<sub>3</sub> (13.66 g, 162.7 mmol) and stirred for 30 min at 0

°C. Acryloyl chloride (5.8 g, 65.1 mmol) was added to the mixture dropwise and the reaction mixture was allowed to reach room temperature overnight. Brine (70 mL) was added and the mixture was extracted with EtOAc (3 × 150 mL). The collected organic fractions were dried with Na<sub>2</sub>SO<sub>4</sub> and the solvent was removed. The crude residue was purified by recrystallization from dichloromethane, yielding the target monomer as a white, crystalline solid (4.1 g, 82 %). <sup>1</sup>H NMR (300 MHz, DMSO-d<sub>6</sub>) δ (ppm): 8.43-8.49 (*d*, NH), 6.05-6.30 (*m*, 2H), 5.60-5.68 (*dd*, 1H), 4.62-4.75 (*ddd*, 1H), 3.26-3.50 (*m*, 2H), 2.40-2.50 (*m*, 1H), 2.0-2.17(*m*, 1H). <sup>13</sup>C NMR (300 MHz, DMSO-d<sub>6</sub>) δ (ppm): 205 (C=O), 165.0 (C=O), 131.5 (CH) 126.6 (CH<sub>2</sub>), 58.2 (CH), 30.6 (CH<sub>2</sub>), 27.5 (CH<sub>2</sub>).

#### Microwave-assisted surface-initiated polymerization of pAHT brush

All μW-SIP reactions were carried out in a mono-mode microwave reactor (CEM Corporation Discover S Class) with a calibrated infrared temperature sensor in constant power mode with simultaneous cooling to maintain the desired temperature. A substrate with the azo-based initiator was placed in a sealed microwave vial and purged with nitrogen. In a separate Schlenk tube, acrylamide homocysteine thiolactone monomer was dissolved in anhydrous dimethyl sulfoxide (DMSO) (0.5 mol/L, 1 mol/L, 1.5 mol/L, and 2 mol/L) and the solution was subjected to three freeze-pump-thaw cycles. For each polymerization, 1.5 mL of the degassed monomer solution was transferred via cannula into the microwave vial containing the substrate. Polymerizations were carried out in the DMSO solution, placed into the microwave reactor, and irradiated at a fixed power of 60 W for 15 min with simultaneous cooling to maintain the reaction temperature at 110 °C. The substrates were sonicated in DMSO for 10 s intervals. After each sonication cycle, the thickness of the brush was measured via ellipsometry. This process was repeated until no change in brush thickness could be measured.

#### PPM of pAHT with amines

The pAHT brushes were post-modified with 4-bromobenzylamine (BBA). A pAHT substrate was placed in a solution of BBA (0.15 mol/L) in DMSO with 3 equivalents of TEA in a sealed test tube under ambient air, temperature and humidity conditions (e.g. without nitrogen purge). The reaction was allowed to react for 15 h. The substrate was then removed, thoroughly rinsed with DMSO, and dried with nitrogen.

#### PPM of thiol pendent pAHT brush with base catalyzed thiol-Michael reactions

All thiol-Michael reactions were performed in septum-sealed test tubes under ambient air, temperature and humidity conditions. Base-catalyzed thiol-Michael reactions were conducted with 1*H*,1*H*-perfluoro-*N*-decyl acrylate (PFDA). Substrates were placed in a 0.15 mol/L solution in acetone

with DBU (0.022 mol/L) for 15 h. The brushes were thoroughly rinsed with acetone, DMSO, and dried with a stream of nitrogen.

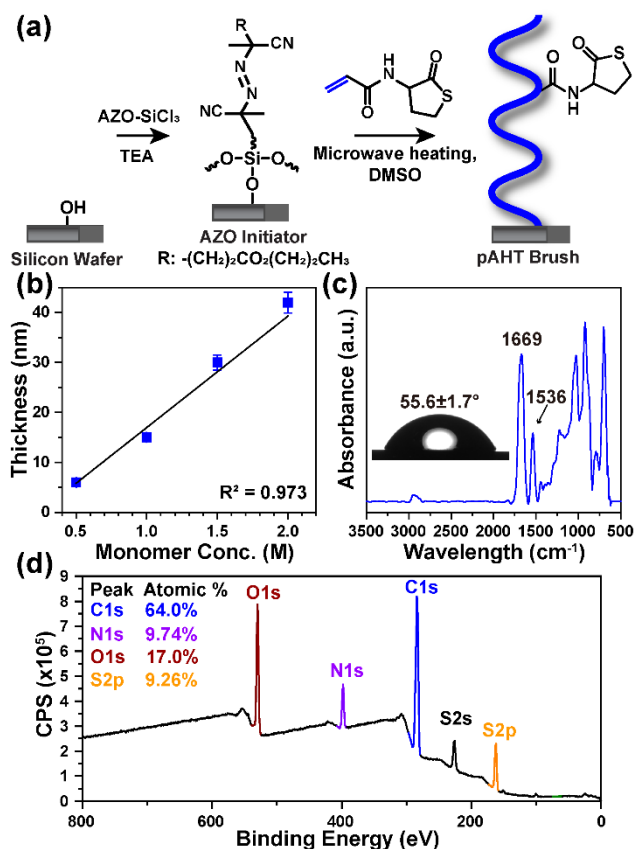
### One-pot double modification reactions

A pAHT substrate was placed in a solution of amine (0.15 mol/L) and acrylate (0.15 mol/L) in DMSO with DBU (0.022 mol/L). Reactions were conducted overnight (approximately 15 h) under ambient conditions to achieve the maximum extent of reaction. Reaction completion was determined by ellipsometry measurement (i.e. no further increase in brush

stamp, the patterned surface was thoroughly rinsed and sonicated in EtOH to remove any physisorbed maleimide.

### Results and Discussion

**Fig. 1a** shows the synthetic strategy for the preparation of poly(acrylamide-homocysteine thiolactone) (pAHT) brushes via microwave-assisted surface-initiated polymerization ( $\mu$ W-SIP) from an azo-based silane initiator on a silicon substrate.<sup>33</sup> The thiolactone acrylamide monomer used for polymerization was prepared by reacting acryloyl chloride with DL-homocysteine thiolactone hydrochloride.<sup>28</sup> <sup>1</sup>H and <sup>13</sup>C NMR spectra are provided in **Fig. S1** and **Fig. S2**, respectively. The average thickness of the azo-based initiator layer was 2.2 nm  $\pm$  0.1 nm as measured by ellipsometry. The pAHT brushes were synthesized via  $\mu$ W-assisted conventional free radical polymerization since it is a simple and well-studied route to design polymer brush surfaces.<sup>33</sup> Polymerizations were carried out in dimethyl sulfoxide (DMSO) under constant microwave power (60 W) with simultaneous cooling to maintain the reaction temperature at 110 °C. **Fig. 1b** shows the relationship between pAHT brush thickness and thiolactone acrylamide monomer concentration obtained at constant time and temperature. Under these conditions, a linear increase in brush thickness with increasing monomer concentration was observed – an expected trend that can be attributed to an increase in brush grafting density.<sup>36, 37</sup> Guo *et al.* previously observed both linear and nonlinear relationships between film thickness and monomer concentration in  $\mu$ W-SIP, depending on the polarity of the monomer and solvent.<sup>33</sup> In the current pAHT/DMSO system, the change in polarity of the monomer/solvent mixture with increasing monomer concentration is negligible, and  $\mu$ W-SIP exhibits the expected linear relationship between brush thickness and monomer concentration. Hereafter, pAHT brushes with a target brush thickness of approximately (30 to 40) nm were synthesized and employed for post-polymerization modification (PPM) reactions. The static water contact angle for the pAHT brush was 56.6°  $\pm$  1.7° (**Fig. 1c**). The chemical composition of the pAHT brush was characterized using gATR-FTIR and XPS. **Fig. 1c** shows the gATR-FTIR spectrum for pAHT with a broad peak at 1669 cm<sup>-1</sup> attributed to an overlap of the carbonyl stretch of the five-membered thiolactone ring and the amide I stretch.<sup>27, 38</sup> The peak at 1536 cm<sup>-1</sup> is indicative of the amide II N-H bending vibration. As shown in **Fig. 1d**, peaks attributed to carbon (C1s, 285 eV), oxygen (O1s, 531 eV), nitrogen (N1s, 400 eV), and sulfur (S2s, 229 eV; S2p 163.4 eV) were observed in the XPS survey spectrum. Quantitative analysis of the pAHT survey spectrum yielded 64.0 atomic % C, 9.74 atomic % N, 17.0 atomic % O, and 9.26 atomic % S – values that are consistent with the expected chemical composition (C<sub>7</sub>N<sub>1</sub>O<sub>2</sub>S<sub>1</sub>, 63.6 atomic % C, 9.10 atomic % N, 18.2 atomic % O, and 9.10 atomic % S) for the pAHT brush. **Fig. S3** shows the high resolution C1s spectrum for the unmodified pAHT brush.



thickness). The

**Fig. 1** (a) Synthesis of pAHT brushes via microwave-assisted surface-initiated polymerization ( $\mu$ W-SIP) (b) Brush thickness versus monomer concentration for  $\mu$ W-SIP of pAHT brushes (DMSO, 60 W, 110 °C, 15 min, mean  $\pm$  S.D., replications = 3). (c) gATR-FTIR and static water contact angle (inset) of the pAHT brush. (d) XPS survey spectrum of the pAHT brush.

brushes were thoroughly rinsed with acetone, DMSO and dried with a stream of nitrogen.

### Post-polymerization modification via microcontact printing

A thiolactone brush was placed in a solution of dansylcadaverine (12 mmol/L) in EtOH with DBU (10 mmol/L) for 15 h to ensure full conversion. Then, a freshly oxidized PDMS stamp was inked with Texas Red® C2 maleimide (25 mmol/L) in EtOH for 1 min, dried with nitrogen, and pressed onto the polymer brush surface for 1 h. After removal of the

### Post-polymerization modification (PPM) of pAHT brush surfaces and sequential thiol-Michael reactions

**Fig. 2a** shows the general scheme for the synthesis of multifunctional homopolymer brushes using sequential or one-pot postmodification strategies. As illustrated in **Fig. 2a**, postmodification with an amine ring-opens the thiolactone exposing a thiol that can be modified via reaction with an electron deficient alkene in sequence or in one-pot.<sup>27</sup> For these experiments, we employed 4-bromobenzylamine (BBA) and 1*H*,1*H*-perfluoro-*N*-decyl acrylate (PFDA) since both modifiers provide elemental tags that can be easily followed via XPS (**Fig. 3a-d**). For sequential modification reactions, the pAHT brush was first exposed to BBA in DMSO for 15 h in the presence of triethylamine (TEA) under ambient conditions (e.g., sealed tube at room temperature without nitrogen purge). The substrates

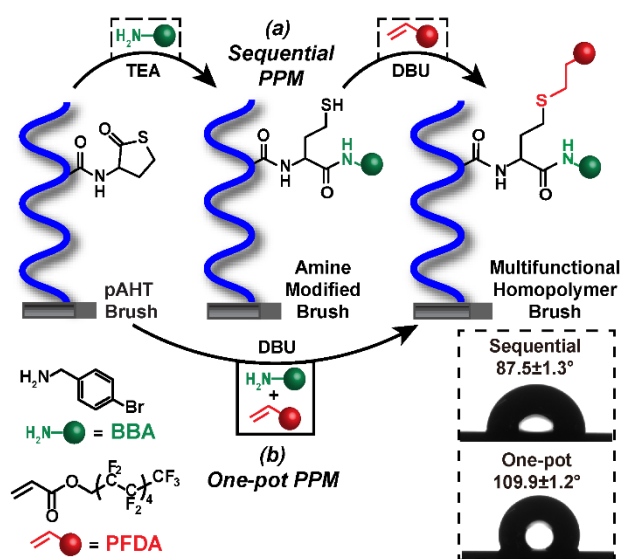


**Fig. 2.** Synthetic strategy to design multifunctional homopolymer brush surfaces via sequential PPM reactions or one-pot PPM with 4-bromobenzylamine (BBA) and 1*H*,1*H*-perfluoro-*N*-decyl acrylate.

were removed from the BBA solution, thoroughly rinsed with DMSO, and quickly transferred to a separate reaction tube containing PFDA and DBU in acetone for 15 h. After exposure to PFDA, the substrates were thoroughly rinsed with acetone and dried under nitrogen. Water contact angle measurements were employed as an initial assessment of the sequential reactions. As expected, surface wettability changed upon modification with BBA and PFDA. For example, the water contact angle (WCA) of the unmodified pAHT brush increased from  $55.6 \pm 1.7^\circ$  to  $87.5 \pm 1.3^\circ$  upon modification due to the incorporation of the hydrophobic bromobenzene and fluorinated functional groups. The modification of pAHT with BBA and FA increases the molecular weight of the polymer repeat unit, resulting in an increase in polymer brush thickness. The thickness values of the pAHT brush before and after PPM were measured using ellipsometry and the results are summarized in **Table 1**. The pAHT brush thickness

increased 130 % from 30 nm to 69 nm upon sequential modification with BBA and FA. Murata and coworkers have demonstrated that the change in brush thickness can be used to determine the conversion of the PPM reaction if brush grafting density and mass density are assumed to remain unchanged during postmodification.<sup>39</sup> However, in the current work, a significant change in mass density of the brush should be expected upon double modification, particularly when incorporating the fluorinated side chains. Since actual mass density values are unknown for the pAHT-BBA-PFDA brush derivatives, we did not attempt to quantify conversion using this approach. Rather, we used XPS and gas cluster ion sputtering (GCIS) to evaluate the conversion and distribution of functional groups throughout the brush resulting from each PPM route.

**Fig. 3a** shows the XPS survey spectra obtained from the pAHT brush interface as a function of depth after sequential modification with BBA and PFDA. Sputtering the brush surface with an argon gas cluster ion beam (6 keV,  $\text{Ar}^+_{300}$ ) provided controlled access to sub-surface layers with good depth resolution while mitigating changes in chemical composition normally associated with single argon ion sputtering sources. At the brush/air interface prior to sputtering (e.g., sputter depth = 0 nm), peaks corresponding to carbon (C1s, 285 eV), oxygen

**Table 1.** Change in brush thickness before and after post-polymerization modification measured via ellipsometry and conversion of sequential and one-pot modified pAHT brush surfaces via XPS.

Modified pAHT Brush	$\Delta$ Thickness (nm)		Thiolactone Conversion XPS (%) <sup>a</sup>	Thiol-Michael Conversion XPS (%) <sup>b</sup>
	Before PPM	After PPM		
pAHT-BBA-PFDA sequential	$30 \pm 0.1$	$69 \pm 0.2$	54.3	10.9
pAHT-BBA-PFDA one-pot	$30 \pm 0.1$	$100 \pm 0.3$	58.7	73.9

<sup>a</sup>Determined from the average [Br3d]/[N1s] atomic ratio throughout the depth profile according to the equation:  $\text{Conv.} = ([\text{Br3d}]/[\text{N1s}])/0.5$ .

<sup>b</sup>Determined from the average [F1s]/[Br3d] atomic ratio throughout the depth profile according to the equation:  $\text{Conv.} = ([\text{F1s}]/[\text{Br3d}])/19$ .

(O1s, 533 eV), and sulfur (S2p, 163 eV) originating from the parent pAHT brush were clearly observed, while the peak for nitrogen (N1s, 400 eV) can be attributed both to the parent pAHT brush and the BBA modifier. The bromine (Br3d) and fluorine (F1s) peaks observed at 70 eV and 698 eV, respectively, confirm successful aminolysis of the pAHT brush with BBA and subsequent Michael addition of the generated thiol to the fluoroacrylate. The spectra from **Fig. 3a** were analyzed after each sputter step to determine the chemical composition of the pAHT-BBA-PFDA brush as a function of depth, as shown in **Fig. 3b**. Sputter time was converted to sputter depth using knowledge of the brush thickness and total sputter time necessary to completely remove the brush

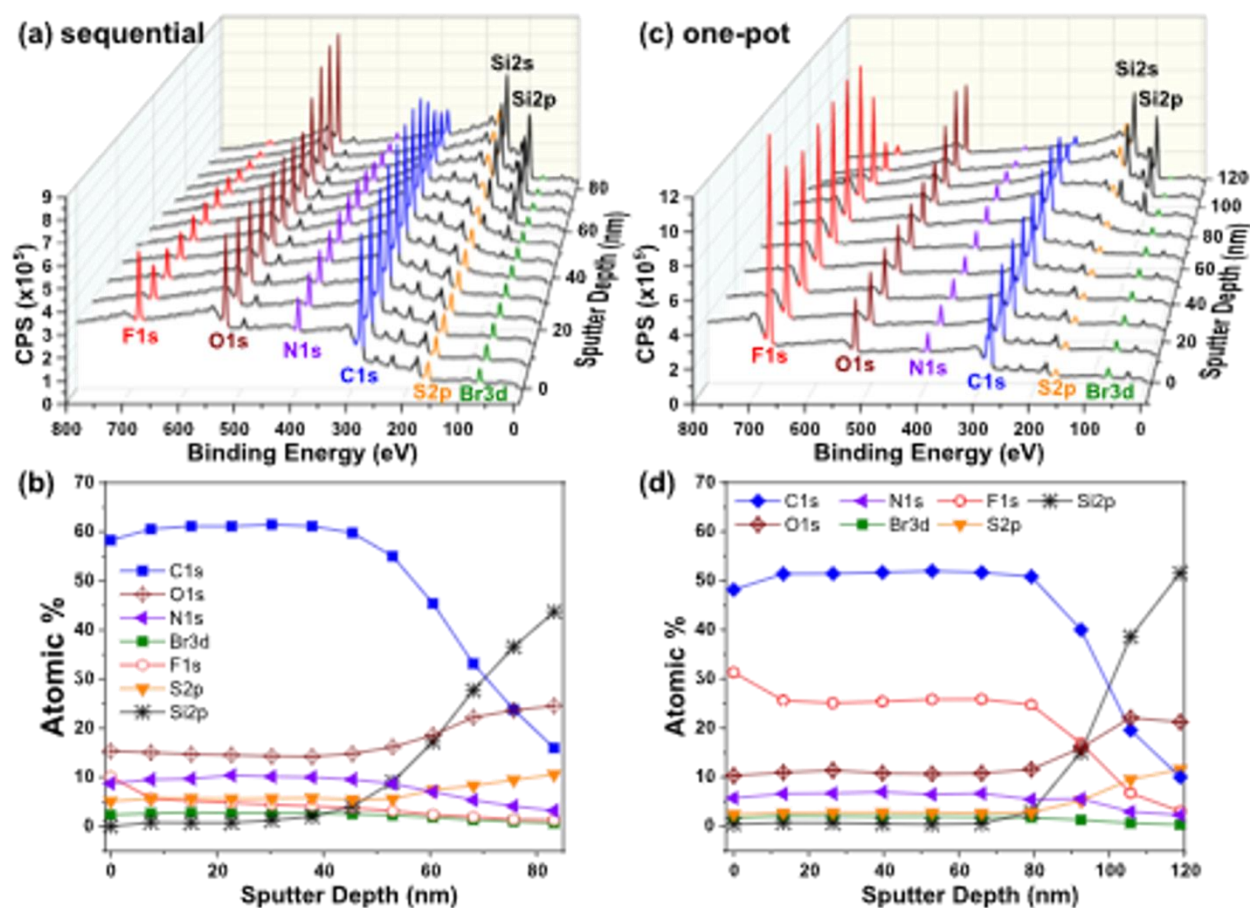


Fig. 3 (a) XPS survey spectra as a function of sputter depth and (b) depth profiles for the sequentially modified pAHT-BBA-PFDA brush. (c) XPS survey spectra as a function of sputter depth and (d) depth profiles for the one-pot modified pAHT-BBA-PFDA brush.

layer. The C1s/Si2p intersection was considered to be the polymer brush/silicon substrate interface; total brush thickness values based on the C1s/Si2p intersection are in good agreement with total brush thickness values obtained from ellipsometry. As shown in Fig. 3b, the C1s, O1s, and S2p concentrations remain relatively constant as a function of sputter depth in the region between 0 nm and 45 nm. These results provide strong evidence of negligible changes in the chemical composition of the brush arising from argon gas cluster ion sputtering. In the near substrate region ( $> 45$  nm), the C1s concentration, as expected, rapidly decreases with a simultaneous increase in the O1s and Si2p concentrations with an observed gradient that is convoluted by the XPS sampling depth ( $\approx 10$  nm). The constant Br3d concentration with depth indicates the first step of the sequential postmodification yields a homogeneous distribution of BBA throughout the brush thickness. The conversion of the thiolactone group was estimated from the [Br3d]/[N1s] ratio – a value that should approach 0.5 at complete aminolysis of the thiolactone. The [Br3d]/[N1s] ratio obtained by averaging the values observed at each depth within the brush was 0.271, which translates to 54.3% thiolactone conversion. While we observed constant bromine concentrations, it is prudent to note that bromine in bromine-containing polymers has been reported to be labile under prolonged X-ray exposure – a degradation process that

would influence our calculated thiolactone conversions.<sup>40</sup> However, quantification from survey spectra allowed us to limit the x-ray exposure time to 220 s per depth profile step to minimize the possible influence of this degradation process. Thus, the less than quantitative conversion observed for BBA modification is likely attributed to the stereo-electronic properties of the primary benzyl amine. In general, similar influences of the amine structure on reactivity have been reported by Espeel *et al.*<sup>27</sup> for the aminolysis of thiolactone. In contrast to the trend observed for bromine, the F1s concentration varies as a function of sputter depth with the highest concentration of fluorine (10 atomic %) present at the brush/air interface followed by a steady decrease to  $< 2$  atomic % at the brush/substrate interface. The enhanced fluorine concentration in the first few nanometers of the pAHT-BBA-PFDA brush can be attributed to segregation of the low surface energy perfluorodecyl side chains to brush/air interface.<sup>41</sup> The conversion of the thiol-Michael reaction was determined from the average [F1s]/[Br3d] ratio measured throughout the depth profile, where a [F1s]:[Br3d] ratio of 19:1 would be expected at full conversion. The observed [F1s]:[Br3d] ratio of 1.91 suggests the thiol-Michael reaction proceeds to only 10.9 % conversion when conducted as a sequential step to the amine-thiolactone reaction. Low conversion for the thiol-Michael reaction is likely due to the

inefficient penetration of the bulky, large molecular mass and non-polar nature of the PFDA molecule into the BBA-modified brush, hindering access to the thiol throughout the brush.<sup>42</sup> Similarly, Klok and coworkers have shown that the size and polarity of the molecules employed in PPM of brush surfaces play important roles in determining conversion and compositional distribution of the postmodified brush.<sup>43,44</sup>

Next, we explored one-pot PPM reactions to produce multifunctional homopolymer brush surfaces. The one-pot reaction, as illustrated in **Fig. 2b**, proceeds analogously to the sequential thiolactone reaction previously described but generates the thiol in situ for immediate reaction with the acrylate, eliminating the intermediate wash/purification step. Specifically, we subjected the pAHT substrate to a homogeneous solution of BBA/PFDA (1:1) and DBU under ambient conditions for 15 h. The one-pot double modification of pAHT with BBA and PFDA resulted in a 230 % increase in thickness from 30 nm for the unmodified pAHT brush to 100 nm for the pAHT-BBA-PFDA brush (Table 1). The significant increase in brush thickness, as compared to the sequential postmodification, points to a more effective immobilization of the two modifiers within the brush. Consequently, the one-pot pAHT-BBA-PFDA brush surfaces were significantly more hydrophobic than the sequential PPM surfaces as indicated by the  $109.9^\circ \pm 1.2^\circ$  water contact angle.

As previously described, XPS with GCIS was employed to characterize the conversion and composition as a function of depth for the one-pot postmodified brush. As shown in **Fig. 3c**, the XPS survey spectrum collected at the brush/air interface (sputter depth = 0 nm) following one-pot PPM is qualitatively similar to the spectrum observed for the sequential PPM reaction, exhibiting both Br3d and F1s peaks indicative of BBA and PFDA immobilization. However, the one-pot surface exhibits a substantial increase in the F1s peak intensity. The chemical composition as a function of depth for the one-pot pAHT-BBA-FA surface is shown in **Fig. 3d**. The through-thickness distribution of bromine is homogeneous – similar to the distribution observed for the sequentially modified brush surface – with an average bromine concentration of 1.87 atomic %. Surface segregation of the perfluoroalkyl side chains at the brush/air interface is again evident in the XPS depth profile with greater than 30 atomic % fluorine at the air interface. The segregation of the perfluorodecyl side chains at the interface explains the significant increase in water contact angle ( $109.9^\circ$ ) observed for the one-pot surfaces, as previously discussed. Except for the brush/air interface, the fluorine is distributed homogeneously throughout the brush thickness until approaching the brush/substrate interface. The one-pot modification results in a thiolactone conversion of 58.7 %, as estimated from the average [Br3d]/[N1s] ratio, and a 73.9 % thiol-Michael conversion as determined from the average [F1s]/[Br3d] ratio. While thiolactone conversions are similar regardless of the PPM route, the one-pot process clearly results in a more effective immobilization and vertical distribution of the fluoroacrylate throughout the brush. The reason for such observation is likely multi-fold. In the one-pot

approach, the unmodified pAHT and, consequently, less sterically crowded brush is swollen simultaneously with BBA and PFDA allowing both modifiers to diffuse more effectively into the surface grafted chains. As a result, the double modification likely proceeds more efficiently due to greater accessibility of the fluoroacrylate to the thiol moieties formed upon ring-opening of the thiolactone. Moreover, the one-pot PPM allows the thiol-Michael reaction to occur immediately upon generation of the thiol without undergoing a wash step, which likely mitigates side reactions typically associated with the thiol functionality (e.g., oxidation, disulfide formation, etc.).

### Patterning pAHT brush surfaces

While the one-pot modification proved to be more effective in immobilizing a high concentration of amine and acrylate modifiers throughout the thickness of the brush, the sequential modification route is ideally suited for the fabrication of micropatterned, multifunctional surfaces. In particular, sequential and/or orthogonal PPM chemistries combined with microcontact printing<sup>19, 45</sup> ( $\mu$ CP) represents a straightforward, low-cost technique to design micropatterned surfaces of interest for a broad range of applications including cell selective

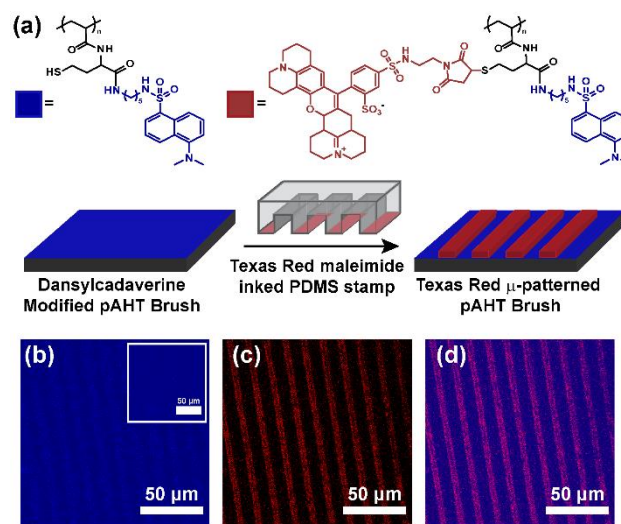


**Fig. 4** Microcontact printing of Texas Red maleimide on the dansylcadaverine-modified pAHT brush. Fluorescent microscopy image of dansylcadaverine-modified pAHT brush and sequential patterning with Texas Red. Excitation of (b) dansylcadaverine at 405 nm (inset image depicts a pAHT brush modified with dansylcadaverine without patterning of Texas Red) (c) Texas Red at 633 nm and (d) both dyes under simultaneous excitation at 405 nm and 633 nm.

adhesion,<sup>46, 47</sup> microfluidics,<sup>48</sup> and organic solar cell devices.<sup>44</sup> Here, we demonstrate the versatility of the thiolactone brush platform to design micropatterned surfaces via reactive  $\mu$ CP using two different fluorescent dyes, one bearing a primary amine and the other a maleimide functionality. First, the pAHT brush was post-modified with dansylcadaverine to install the dye and liberate the thiol moiety. After thoroughly rinsing, excitation of the surface at 405 nm revealed a homogeneous fluorescence from the dansylcadaverine-modified pAHT brush

(Fig. 4b, inset). Next, a PDMS stamp (5  $\mu\text{m}$  lines spaced by 10  $\mu\text{m}$ ) was inked with a 10 mM solution of Texas Red C2 maleimide in EtOH, dried with nitrogen, and placed in contact with the dansylcadaverine-modified pAHT brush surface for 1 h (Fig. 4a). After functionalization via  $\mu\text{CP}$ , the substrate was sonicated in EtOH and the patterned surface was investigated using confocal microscopy. Excitation of the micropatterned surface at 405 nm again revealed the blue fluorescence originating from the immobilized dansylcadaverine with the presence of a faint line pattern (Fig. 4b). The faint patterned lines observed in Fig. 4b under 405 nm excitation are likely due to secondary excitation of Texas Red by the dansylcadaverine fluorescence, which overlaps with the excitation spectrum for Texas Red. Changing the excitation wavelength to 633 nm to address the Texas Red dye resulted in the observation of red fluorescence in 5  $\mu\text{m}$  stripes each separated by 10  $\mu\text{m}$  (Fig. 4c). When both dyes were excited simultaneously, the surface exhibits the expected line pattern that reproduces the micropattern stamp with high fidelity (Fig. 4d).

## Conclusions

In this work, we have demonstrated the synthesis of poly(acrylamide-homocysteine thiolactone) brushes via surface-initiated polymerization. Post-polymerization modification of this versatile thiolactone platform using sequential and one-pot amine-thiol-ene conjugation reactions with bromobenzyl amine and 1H,1H-perfluoro-N-decyl acrylate provided facile access to multifunctional homopolymer brush surfaces. Depth profile experiments conducted via XPS and argon gas cluster ion sputtering provided insight into the efficiency of the two PPM routes (e.g., sequential versus one-pot reactions), particularly in terms of double conjugation conversion and through-thickness brush composition. The depth profile of the sequentially modified surface showed that the aminolysis reaction with BBA proceeded homogeneously throughout the brush (albeit at a modest 54 % conversion), but subsequently hindered the progression of the thiol-Michael reaction with PFDA (11 % conversion). In contrast, simultaneously exposing the pAHT brush to BBA and PFDA via the one-pot approach allowed both modifiers to readily diffuse into the brush resulting in a more efficient double conjugation (59 % aminolysis conversion, 74% thiol-Michael conversion). Despite suffering lower post-polymerization efficiency, the sequential modification route readily serves as a modular platform to design complex and well-defined micropatterned surfaces when combined with reactive  $\mu\text{CP}$ . Ultimately, polymer brushes carrying pendent thiolactone functional groups provide an attractive surface engineering approach for the design of multifunctional brush architectures using a wide array of amines and thiol-reactive modifiers.

## Conflicts of interest

There are no conflicts to declare.

## Acknowledgements

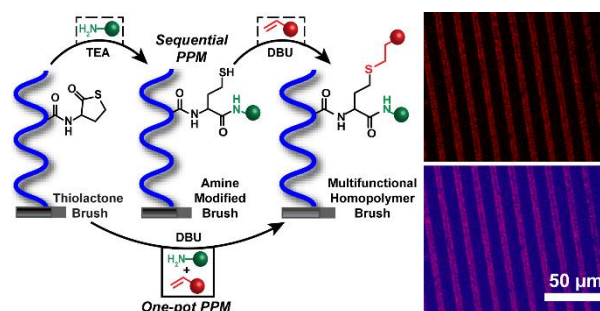
This work was supported in part by the American Chemical Society Petroleum Research Fund (PRF# 55833-ND7). CMR acknowledges support from the NSF Graduate Research Fellowship Program (DGE-1445151) and traineeship support from the NSF NRT "Interface" program (DGE-1449999) through the University of Southern Mississippi. The purchase of the XPS instrumentation was supported by the NSF Major Research Instrumentation program (DMR-1726901). Official contribution of the National Institute of Standards and Technology; not subject to copyright in the United States.

## Notes and references

1. S. Krishnan, C. J. Weinman and C. K. Ober, *J. Mater. Chem.*, 2008, **18**, 3405-3413.
2. B. Xu, C. Feng, J. Hu, P. Shi, G. Gu, L. Wang and X. Huang, *ACS Appl. Mater. Interfaces*, 2016, **8**, 6685-6692.
3. A. de los Santos Pereira, T. Riedel, E. Brynda and C. Rodriguez-Emmenegger, *Sensors Actuat. B Chem.*, 2014, **202**, 1313-1321.
4. O. Wiarachai, T. Vilaivan, Y. Iwasaki and V. P. Hoven, *Langmuir*, 2016, **32**, 1184-1194.
5. R. R. Bhat, B. N. Chaney, J. Rowley, A. Liebmann-Vinson and J. Genzer, *Adv. Mater.*, 2005, **17**, 2802-2807.
6. Y. Deng, J. Z. Zhang, Y. Li, J. Hu, D. Yang and X. Huang, *J. Polym. Sci. A: Polym. Chem.*, 2012, **50**, 4451-4458.
7. Y. Li, Z. Jian, M. Lang, C. Zhang and X. Huang, *ACS Appl. Mater. Interfaces*, 2016, **8**, 17352-17359.
8. Y. Yang, J. Wang, J. Zhang, J. Liu, X. Yang and H. Zhao, *Langmuir*, 2009, **25**, 11808-11814.
9. W. Guo, C. M. Reese, L. Xiong, P. K. Logan, B. J. Thompson, C. M. Stafford, A. V. Ievlev, B. S. Lokitz, O. S. Ovchinnikova and D. L. Patton, *Macromolecules*, 2017, **50**, 8670-8677.
10. H. Huang, J. Y. Chung, A. J. Nolte and C. M. Stafford, *Chem. Mater.*, 2007, **19**, 6555-6560.
11. N. Ayres, *Polym. Chem.*, 2010, **1**, 769-777.
12. R. Barbey, L. Lavanant, D. Paripovic, N. Schüwer, C. Sugnaux, S. Tugulu and H.-A. Klok, *Chem. Rev.*, 2009, **109**, 5437-5527.
13. R. M. Arnold, N. E. Huddleston and J. Locklin, *J. Mater. Chem.*, 2012, **22**, 19357-19365.
14. C. J. Galvin and J. Genzer, *Prog. Polym. Sci.*, 2012, **37**, 871-906.
15. K. A. Günay, N. Schüwer and H.-A. Klok, *Polym. Chem.*, 2012, **3**, 2186-2192.
16. M. A. Gauthier, M. I. Gibson and H. A. Klok, *Angew. Chem. Int. Ed.*, 2009, **48**, 48-58.
17. K. A. Gunay, P. Theato and H. A. Klok, *J. Polym. Sci. A: Polym. Chem.*, 2013, **51**, 1-28.
18. R. M. Arnold, D. L. Patton, V. V. Popik and J. Locklin, *Acc. Chem. Res.*, 2014, **47**, 2999-3008.
19. M. Buhl, M. Tesch, S. Lamping, J. Moratz, A. Studer and B. J. Ravoo, *Chem. Euro. J.*, 2017, **23**, 6042-6047.
20. M. Dübner, V. J. Cadarso, T. N. Gevrek, A. Sanyal, N. D. Spencer and C. Padeste, *ACS Appl. Mater. Interfaces*, 2017, **9**, 9245-9249.
21. S. B. Rahane, R. M. Hensarling, B. J. Sparks, C. M. Stafford and D. L. Patton, *J. Mater. Chem.*, 2012, **22**, 932-943.

22. T. Kubo, K. C. Bentz, K. C. Powell, C. A. Figg, J. L. Swartz, M. Tansky, A. Chauhan, D. A. Savin and B. S. Sumerlin, *Polym. Chem.*, 2017, **8**, 6028-6032.
23. T. Kubo, C. P. Easterling, R. A. Olson and B. S. Sumerlin, *Polym. Chem.*, 2018, **9**, 4605-4610.
24. M. Lillethorup, K. Shimizu, N. Plumeré, S. U. Pedersen and K. Daasbjerg, *Macromolecules*, 2014, **47**, 5081-5088.
25. P. Espeel, F. Goethals and F. E. Du Prez, *J. Am. Chem. Soc.*, 2011, **133**, 1678-1681.
26. P. Espeel, F. Goethals, M. M. Stamenović, L. Petton and F. E. Du Prez, *Polym. Chem.*, 2012, **3**, 1007-1015.
27. P. Espeel, F. Goethals, F. Driessen, L.-T. T. Nguyen and F. E. Du Prez, *Polym. Chem.*, 2013, **4**, 2449-2456.
28. S. Reinicke, P. Espeel, M. M. Stamenović and F. E. Du Prez, *ACS Macro Lett.*, 2013, **2**, 539-543.
29. S. Belbekhouche, S. Reinicke, P. Espeel, F. E. Du Prez, P. Eloy, C. Dupont-Gillain, A. M. Jonas, S. Demoustier-Champagne and K. Glinel, *ACS Appl. Mater. Interfaces*, 2014, **6**, 22457-22466.
30. P. Espeel and F. E. Du Prez, *Eur. Polym. J.*, 2015, **62**, 247-272.
31. C. Chattaway, S. Belbekhouche, F. E. Du Prez, K. Glinel and S. Demoustier-Champagne, *Langmuir*, 2018, **34**, 5234-5244.
32. A. J. Satti, P. Espeel, S. Martens, T. Van Hoeylandt, F. E. Du Prez and F. Lynen, *J. Chromatogr. A*, 2015, **1426**, 126-132.
33. W. Guo, R. M. Hensarling, A. L. LeBlanc, E. A. Hoff, A. D. Baranek and D. L. Patton, *Macromol. Rapid Commun.*, 2012, **33**, 863-868.
34. D. L. Patton, K. A. Page, E. A. Hoff, M. J. Fasolka and K. L. Beers, *Polym. Chem.*, 2012, **3**, 1174-1181.
35. D. L. Patton, K. A. Page, C. Xu, K. L. Genson, M. J. Fasolka and K. L. Beers, *Macromolecules*, 2007, **40**, 6017-6020.
36. O. Prucker and J. Rühe, *Langmuir*, 1998, **14**, 6893-6898.
37. C. Schuh and J. Rühe, *Macromolecules*, 2011, **44**, 3502-3510.
38. S. Montolio, O. Zagorodko, R. Porcar, M. Isabel Burguete, S. V. Luis, H. Tenhu and E. García-Verdugo, *Polym. Chem.*, 2017, **8**, 4789-4797.
39. H. Murata, O. Prucker and J. Rühe, *Macromolecules*, 2007, **40**, 5497-5503.
40. R. J. Sheridan, S. V. Orski, S. Muramoto, C. M. Stafford and K. L. Beers, *Langmuir*, 2016, **32**, 8071-8076.
41. R. R. Thomas, D. R. Anton, W. F. Graham, M. J. Darmon, B. B. Sauer, K. M. Stika and D. G. Swartzfager, *Macromolecules*, 1997, **30**, 2883-2890.
42. W. Guo, L. Xiong, C. M. Reese, D. V. Amato, B. J. Thompson, P. K. Logan and D. L. Patton, *Polym. Chem.*, 2017, **8**, 6778-6785.
43. R. Barbey, V. Laporte, S. Alnabulsi and H.-A. Klok, *Macromolecules*, 2013, **46**, 6151-6158.
44. N. Schüwer, T. Geue, J. P. Hinestrosa and H.-A. Klok, *Macromolecules*, 2011, **44**, 6868-6874.
45. B. D. Gates, Q. Xu, M. Stewart, D. Ryan, C. G. Willson and G. M. Whitesides, *Chem. Rev.*, 2005, **105**, 1171-1196.
46. A. H. Broderick, S. M. Azarin, M. E. Buck, S. P. Palecek and D. M. Lynn, *Biomacromolecules*, 2011, **12**, 1998-2007.
47. Z. Tang, Y. Akiyama and T. Okano, *Polymers*, 2012, **4**, 1478-1498.
48. K. Tsougeni, P. S. Petrou, D. P. Papageorgiou, S. E. Kakabakos, A. Tserepi and E. Gogolides, *Sensors Actuat. B Chem.*, 2012, **161**, 216-222.

## TOC Graphic



**TOC caption:** Polymer brushes carrying pendent thiolactone functional groups were explored for the design of multifunctional homopolymer brush architectures using sequential and one-pot postpolymerization strategies.